LIMNOLOGY and OCEANOGRAPHY

ASLO

Limnol. Oceanogr. 68, 2023, 56–69

doi: 10.1002/lno.12248

Surface productivity gradients govern changes in the viability of deep ocean prokaryotes across the tropical and subtropical Atlantic

Markel Gómez-Letona,[1*] **Javier Arístegui**,[1*] **Nauzet Hernández-Hernández**,[1] **María Pérez-Lorenzo**,[2] **Xosé Antón Álvarez-Salgado**,[3] **Eva Teira**,[2] **Marta Sebastián**[4]

[1]Instituto de Oceanografía y Cambio Global, Universidad de Las Palmas de Gran Canaria, Las Palmas, Spain
[2]Centro de Investigación Mariña da Universidade de Vigo (CIM-UVigo), Departamento de Ecología y Biología Animal, Universidade de Vigo, Vigo, Spain
[3]Instituto de Investigacións Mariñas (IIM), CSIC, Vigo, Spain
[4]Department of Marine Biology and Oceanography, Institut de Ciències del Mar (ICM), CSIC, Barcelona, Spain

Abstract

Prokaryotes represent a major fraction of marine biomass and play a key role in the global carbon cycle. We studied the vertical profiles (0–3500 m) of abundance, viability, and activity of prokaryotic communities along a productivity gradient in the subtropical and tropical Atlantic to assess whether there is a vertical linkage between surface productivity regimes and deep ocean prokaryotic communities. We found that latitudinal changes in the vertical patterns of cytometric variables were coupled with surface productivity: higher prokaryotic abundances and viabilities, and smaller cell sizes were observed below highly productive surface waters, an effect reaching down to the bathypelagic layer. Leucine uptake rates in deep waters showed no clear relationship with surface productivity. Changes in resource and energy allocation to growth vs. maintenance in hostile environments, cell-size-dependent metabolic requirements, and variability in leucine-to-carbon conversion may all be part of the array of factors involved in controlling the prokaryotic activity patterns that were measured. Our work adds to the recent findings that highlight the importance of vertical connectivity for prokaryotic communities in the dark ocean and unveils a remarkable impact of surface conditions in the viability of deep ocean prokaryotes. This is a key aspect when considering metabolic rates of prokaryotic communities in the bathypelagic realm.

Prokaryotes represent a key component of marine ecosystems. At abundances typically ranging from thousands to millions of cells per milliliter, they conform a major fraction of the biomass of marine organisms (Whitman et al. 1998; Bar-On et al. 2018) and make use of a wide variety of energy and carbon sources (Moran 2015), driving global biogeochemical cycles. While prokaryotes are distributed along the entire water column, their abundance and activity are not constant. Epipelagic communities exhibit markedly higher abundances, biomass and production rates, lower percentages of cells with high nucleic acid content, and smaller cell sizes than those in meso- and bathypelagic waters (Arístegui et al. 2009). Nonetheless, given the vast volume of water encompassed by the dark ocean, prokaryotes in this realm are responsible for 75% and 50% of the ocean's prokaryotic biomass and production, respectively (Arístegui et al. 2009), underlining the importance of considering dark ocean communities when studying the carbon cycle in the ocean.

In surface open-ocean waters, the organic matter consumed by prokaryotes stems either from in situ primary production or from lateral advection from coastal adjacent regions (Santana-Falcón et al. 2020). In the dark ocean, however, while chemolithoautotrophy (Baltar et al. 2010*c*) or carbon excretion by diel vertical migrants (Steinberg et al. 2008) may significantly contribute as carbon sources, the vertical flux of particles that escape remineralization in the photic layer is assumed to be the main source of organic carbon (Boyd et al. 2019). These particles have diverse origins: they may consist of phytoplankton cells (Guidi et al. 2009), zooplankton fecal pellets

*Correspondence: markel.gomezletona@ulpgc.es and javier.aristegui@ulpgc.es

Additional Supporting Information may be found in the online version of this article.

Author Contribution Statement: J.A., M.S., and M.G.-L. contributed to the study's conception. All authors contributed to data acquisition and analysis. M.G.-L. wrote the manuscript with contributions from M.S., J.A., E.T., and X.A.A.-S. All authors approved the final submitted manuscript.

(Turner 2015), or polymer gel structures (Verdugo 2012). Not only they are a source of organic matter to deep ocean layers, but also act as vectors that vertically connect prokaryotic communities (Mestre et al. 2018; Ruiz-González et al. 2020). However, a link between surface productivity or particle flux and prokaryotic biomass or production in the dark ocean has not always been found (Arístegui et al. 2009 and references therein; Herndl and Reinthaler 2013). Episodic vertical inputs and lateral advection of organic matter have been suggested as possible explanations for this lack of relationship (Yokokawa et al. 2013; Smith et al. 2018).

Alternatively, the time of response of deep ocean prokaryotes to organic matter inputs might vary between and within communities. This could be due to changes in the physiological status of individual cells, which can range from death, to limited activity or active growth (del Giorgio and Gasol 2008). For instance, the percentage of viable prokaryotes within a community (those with intact cell membranes, a measure of their physiological status) in epipelagic waters has been previously associated with the release of organic matter by senescent phytoplankton (Lasternas and Agustí 2014), although it is not known if dark ocean communities respond in a similar way. Viability estimates in meso- and bathypelagic waters are scarce, but point to a reduction of viability with depth, from > 80% in surface waters down to 10–40% (Gasol et al. 2009; Baltar et al. 2012), probably related to the more adverse conditions found in the dark realm (high pressure, low temperature, reduced organic carbon availability). Thus, assessing what drives the variability in the physiological status of dark ocean communities is key to adequately understand their bulk metabolic rates, including their response (or lack of response) to the vertical flux of organic matter.

To study the potential link between the physiological status of dark ocean prokaryotes and surface productivity, we studied prokaryotic communities along a section crossing the tropical and subtropical Atlantic Ocean, from the surface down to 3500 m. The studied region is complex, with a considerable number of currents (Brandt et al. 2008) and water masses (Pérez et al. 2001; Álvarez et al. 2014). Remarkably, it presents a strong surface productivity gradient, comprising both oligotrophic waters and areas directly under the influence of the Northwest African upwelling system, where high export rates of sinking particles have been reported (Fischer et al. 2020). We determined the abundance and viability of prokaryotic communities, estimated their cell size, and measured leucine incorporation rates, to assess whether these variables were affected by changes in surface productivity, evaluating the degree to which the standing stock and, more importantly, the metabolic status of deep prokaryotic communities were linked to epipelagic waters.

Methods

Study area

During the MAFIA cruise (*Migrants and Active Flux In the Atlantic Ocean*, April 2015, on board R/V Hespérides) seawater samples were collected at 13 stations along a section crossing a productivity gradient in the subtropical and tropical Atlantic (13°S–27°N, Fig. 1). Sample collection was performed using a General Oceanics oceanographic rosette equipped with PVC Niskin bottles alongside a Seabird 911-plus CTD, a Seapoint Chlorophyll Fluorometer and a Seabird-43 Dissolved Oxygen Sensor. The chlorophyll a (Chl *a*) values provided by the fluorometer were based on the factory calibration.

Prokaryotic cell abundance, size, and viability

Seawater samples for measuring the abundance of prokaryotes were collected in all stations at 22 depths, from surface down to 3500 m (or bottom, when above this depth). Samples were collected into 1.2-mL cryovials, fixed with a 2% final concentration of formaldehyde, after keeping them 30 min at 4°C, and then stored frozen in liquid nitrogen. After 24 h, they were analyzed in an FACSCalibur (Becton-Dickinson) flow cytometer. Subsamples (400 μL) were stained with 4 μL of the fluorochrome SYBR Green I (Molecular Probes) diluted in dimethyl sulfoxide (1 : 10). Fluorescent beads (1 μm, Polysciences) were added for internal calibration (10^5 mL^{-1}). High and low nucleic acid content (HNA and LNA, respectively) prokaryotic cells were identified in green vs. red fluorescence and green fluorescence vs. side scatter cytograms. Average cell volumes (in μm^3) were estimated from side scatter based on the relationship described by Calvo-Díaz and Morán (2006) assuming spherical shape:

$$\text{Cell volume} = \frac{4}{3} \times \pi \times \left[\frac{0.908 + 0.34 \times \log_{10}(\text{Relative side scatter})}{2} \right]^3$$

Where *Relative side scatter* is the (side scatter of prokaryotes)/(side scatter of beads) ratio. An in-house calibration was applied to transform relative side scatter values from Polysciences-bead-referenced to Molecular-Probes-bead-referenced ($[\text{Relative side scatter}]_{MP} = 2.201 \times [\text{Relative side scatter}]_{PS}$). Prokaryotic biomass was then estimated applying the volumetric relationship (Norland 1993)

$$\text{pg C cell}^{-1} = 0.12 \times (\text{cell volume})^{0.7}$$

Prokaryotic cell viability was studied as an approach to assess the physiological status of cells, classifying them as viable (intact cell membrane; live and potentially active) and nonviable (compromised cell membrane; dead or injured). Viability was determined by nucleic-acid double-staining using SYBR Green I and propidium iodide (Falcioni et al. 2008) following Baltar et al. (2010*a*). Stained unfixed samples were analyzed in the cytometer immediately after sample collection from the Niskin bottles to minimize membrane damage by depressurization. The effect of depressurization on cell membranes has been observed to be minimal within the first few hours,

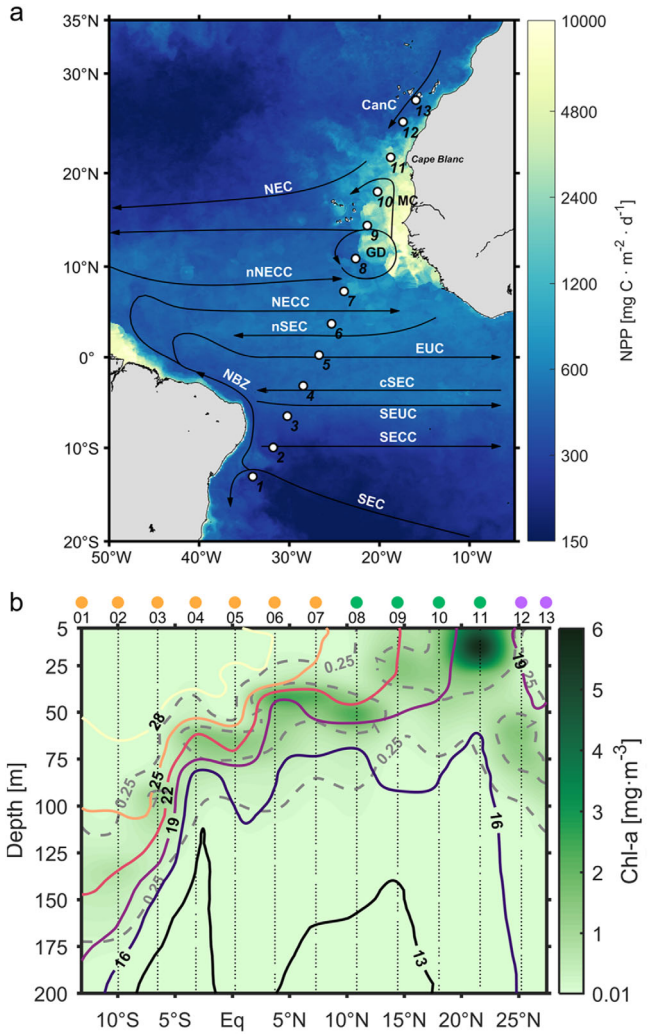

Fig. 1. Surface productivity during the MAFIA cruise. (**a**) Sampling stations (1–13). The underlying color map represents net primary production estimates for April 2015 (Eppley-VGPM model, MODIS dataset, Oregon State University, http://sites.science.oregonstate.edu/ocean.productivity/). Major ocean currents in the study region (based on Stramma and Schott 1999 and Brandt et al. 2008) are also displayed: CanC = canary current; NEC = north equatorial current; MC = Mauritanian current; GD = Guinea dome; nNECC = northern north equatorial counter current; NECC = north equatorial counter current; nSEC = northern south equatorial current; EUC = equatorial under current; NBZ = North Brazil current; cSEC = central south equatorial current; SEUC = south equatorial under current; SECC = south equatorial counter current; SEC = south equatorial current. (**b**) Chl *a* concentrations (derived from the CTD fluorometer) and potential temperature isotherms (in °C) in the epipelagic layer along the cruise section. Dashed isolines represent Chl *a* concentrations. Dots on top of station numbers represent station groups: "South" (light orange), Guinea Dome-Cape Blanc ("Guinea Dome-Cape Blanc," green), "North" (violet).

especially if the pressure change is done gradually (Park and Clark 2002; Quéric et al. 2004), as it occurs during the rosette retrieval. Viable and non-viable cell populations were identified in green vs. red fluorescence cytograms. The dataset comprising all cytometry results is available in the PANGAEA repository (pangaea.de) under accession number 943414 (Gómez-Letona et al. 2022*a*,*b*).

Prokaryotic activity

Prokaryotic activity was quantified by measuring tritiated leucine incorporation (Kirchman et al. 1985). The centrifugation and filtration methods (Smith and Azam 1992) were applied for samples collected at ≤ 1000 m and > 1000 m depth, respectively. For the centrifugation method, 1 mL of sample was incubated (3–12 h, four replicates and two blanks) with a final leucine concentration of 20 nM. For epipelagic samples (≤ 150 m) this was done with lukewarm leucine (1 : 10 dilution) and for mesopelagic samples (300–1000 m) with hot leucine (1 : 1 dilution). For the filtration method, samples of 40 mL were incubated (12–24 h, two replicates and one blank) with a final concentration of 5 nM (hot leucine, 1 : 1). The employed leucine had a specific activity of 112 Ci mmol^{-1}. *See* Supplementary Fig. S1 for a comparison of results obtained through both methods. Incubations were stopped by adding trichloroacetic acid to a final concentration of 5% for the centrifugation method and formaldehyde to a final concentration of 2% for the filtration method. For the latter, filters were then washed twice with trichloroacetic acid (50%). After centrifugation/filtration, a scintillation cocktail was added to the samples and the disintegrations per minute (dpm) were computed employing a Wallac scintillation counter with quenching correction, using an external standard. Dpm were converted to leucine incorporation rates based on the equation

$$\text{mmol Leu L}^{-1}\,\text{h}^{-1} = 4.5^{-13} \times \left(\text{dpm}_{\text{sample}} - \text{dpm}_{\text{blank}}\right) \times \text{SA}^{-1} \times T^{-1} \times V^{-1}$$

where 4.5^{-13} is the number of curies per dpm (constant), SA is the specific activity of the leucine solution, T is the incubation time in hours, and V is the incubation volume in liters. Specific leucine incorporation rates per viable cell were estimated making use of the results from the nucleic-acid double-staining protocol (see above). The leucine incorporation data is available in the PANGAEA repository (pangaea.de) under accession number 943414 (Gómez-Letona et al. 2022*a*,*b*).

Multiparameter water mass analysis

The contribution of water masses in each sample deeper than 100 m was objectively quantified using of the optimum multiparameter analysis described in detail in Gómez-Letona et al. (2022*d*). Briefly, based on previous hydrographic studies in the area (Álvarez et al. 2014; Catalá et al. 2015), 12 source water types were identified in the collected water samples (Supplementary Fig. S2; Supplementary Table S1): Salinity Maximum Water, Madeira Mode Water, Equatorial Water, Eastern North Atlantic Central Water of 15°C and 12°C,

Subpolar Mode Water, Mediterranean Water, Antarctic Intermediate Water of 5°C and 3.1°C, Circumpolar Deep Water and North Atlantic Deep Water of 4.6°C and 2°C. The contribution of each of them to each sample is quantified by solving a set of four conservative linear mixing equations defined by potential temperature (θ), salinity (S), silicate (SiO_4H_4), and the conservative NO tracer ($= O_2 + R_N{\cdot}NO_3$ with $R_N = 9.3$; Broecker 1974; Álvarez et al. 2014) (Table S2), plus a fifth equation that constrained the sum of the water mass contributions to 1. The resulting distribution of water masses in the study area can be found in Supplementary Fig. S2. Archetype values of physical and biogeochemical variables were estimated for each water mass as weighed means based on the contribution of water masses to each sample (Álvarez-Salgado et al. 2013; Catalá et al. 2015).

Statistical analyses

All statistical analyses were carried out in R (v. 3.6.0, R Core Team 2019). To assess the relationship between surface productivity and the prokaryotic community, linear regressions were calculated for cytometric variables and leucine incorporation rates using surface Chl *a* (average within the upper 20 m) as the independent variable. Regressions were estimated separately for epipelagic (0–200 m), mesopelagic (200–1000 m), and bathypelagic (1000–3000 m) layers, using averaged (for HNA%, cell size, viability, and cell-specific leucine incorporation) and integrated (for abundances and bulk leucine incorporation) values of the dependent variables for each depth range. Integrated values were calculated by multiplying data values by the distance in meters between data points, based on an interpolated grid (see Figs. 2, 4) estimated with DIVA (Troupin et al. 2012) in Matlab (R2017a) (see Supporting Methods for details). This dataset is available in the PANGAEA repository (pangaea.de) under accession number 943416 (Gómez-Letona et al. 2022*a*,*c*). Regressions of leucine incorporation vs. cell size were also calculated.

Log–log linear regressions of prokaryotic abundances and leucine incorporation vs. depth were estimated (including samples of ≥ 10 m depth) to evaluate vertical trends. Regressions were estimated both jointly for the entire dataset and grouping stations based on surface productivity gradients (see section Surface productivity gradient along the cruise section for details): Stats. 1–7, with low surface Chl *a* values, were grouped as "South"; Stas. 8–11, with high Chl *a* values, as "Guinea Dome-Cape Blanc"; and Stas. 12–13, again with low Chl *a* values, as "North."

Results

Surface productivity gradient along the cruise section

The oceanographic section crossed regions with markedly different productivity regimes, as depicted by net primary production estimates and Chl *a* patterns (Fig. 1). Stations in the southern end of the section (1–2), off the coast of Brazil, presented conditions typically associated to oligotrophic waters, with low surface Chl *a* values (0.03–0.07 mg m^{-3}) and a deep chlorophyll maximum (DCM) located at ~ 135 m depth, showing concentrations that barely exceeded 0.5 mg m^{-3}. Despite consistently showing low surface Chl *a* values, Stas. 3–7 presented an increasing trend, from 0.04–0.06 mg m^{-3} at Sta. 3 to 0.11–0.19 mg m^{-3} at Sta. 7. A parallel shoaling and strengthening of the DCM were evident, from 95 m (1.2 mg m^{-3}) at Sta. 3 to 40 m (2.3 mg m^{-3}) at Sta. 7. At Stas. 8–11, surface Chl *a* concentrations markedly increased, transitioning to highly productive waters: from 0.25–1.3 mg m^{-3} in the Guinea Dome area (Stas. 8–9) to 1.4–1.5 mg m^{-3} at Sta. 10 and 4.8–5.9 mg m^{-3} at Cape Blanc (Sta. 11). These stations showed the shallowest DCMs, with Cape Blanc peaking at 15 m and 5.9 mg m^{-3}. Entering the oligotrophic Canary Current, Stas. 12–13 presented a sharp decrease in surface Chl *a* values (0.19–0.24 mg m^{-3}), while the DCM became deeper and weaker (85 m and 1.1 mg m^{-3} at Sta. 13).

Spatial distribution patterns of cytometric signatures

Prokaryotic abundances (Fig. 2a) showed decreasing numbers of cells with depth in all stations (log–log slope vs. depth $= -0.816 \pm 0.035$; Table 1). Concentrations in epipelagic waters were always above 10^5 cells mL^{-1} with peaks exceeding 10^6 cells mL^{-1} in surface samples in Stas. 6, 9, 10 and, especially, 11 (Cape Blanc area), where concentrations reached 2×10^6 cell mL^{-1}. Despite the widespread decrease with depth, prokaryotic abundances displayed latitudinal differences in the dark ocean too: increasing values were observed from the tropical South Atlantic (10^5 cells mL^{-1} at ~ 300 m and $< 2.5 \times 10^4$ cells mL^{-1} below 1000–1500 m) to the Cape Blanc area (10^5 cells mL^{-1} at ~ 700 m and $> 2.5 \times 10^4$ cells mL^{-1} in the entire water column). Indeed, there was a significantly positive relationship between surface Chl *a* concentrations and integrated prokaryotic abundances in the epipelagic, mesopelagic, and bathypelagic layers (Fig. 3a; Supplementary Table S2). These gradients were reflected in changes in log–log slopes ("South" $= -0.823 \pm 0.042$ vs. "Guinea Dome-Cape Blanc" $= -0.783 \pm 0.045$; Supplementary Fig. S3; Table 1) and the archetype prokaryotic cell abundances of the water masses (Table 2; *see* Supplementary Fig. S2 for a scheme of the distribution of water masses along the section): the Salinity Maximum Water (134 ± 11 m) in the southern part of the section, presented markedly lower values ($27.4 \pm 3.2 \times 10^4$ cells mL^{-1}) than the Madeira Mode Water (130 ± 17 m; $38.0 \pm 5.6 \times 10^4$ cells mL^{-1}), found in the northern part. Similarly, the Antarctic Intermediate Water of 5°C (713 ± 47 m) showed lower archetype prokaryotic abundances than the Subpolar Mode Water (696 ± 56 m), the former presenting $5.8 \pm 0.5 \times 10^4$ cells mL^{-1} and the latter $9.5 \pm 0.8 \times 10^4$ cells mL^{-1}. Bathypelagic water masses were distributed along the entire section and, thus, their differences were only depth-dependent (Table 2), but intra-water mass latitudinal changes were evident (Figs. 2a, S2).

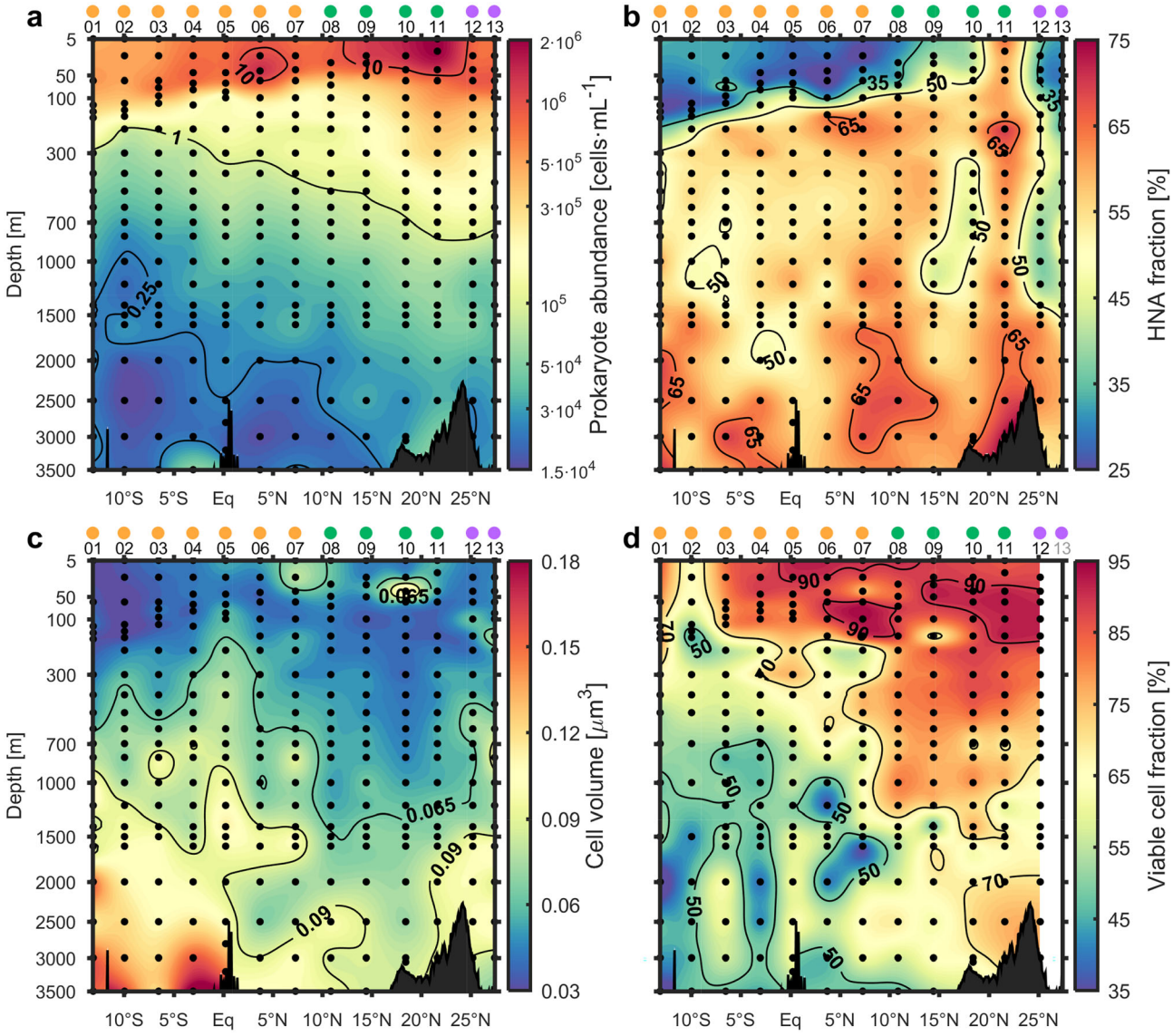

Fig. 2. Characterization of the prokaryotic community by flow cytometry. (**a**) Total prokaryotic cell abundance. Labels on contour lines are in 10^5. (**b**) Fraction of the community represented by HNA prokaryotes. (**c**) Mean volume of prokaryotic cells. (**d**) Viability of prokaryotic cells as per nucleic-acid double-staining (see Methods section). Black dots represent locations of collected samples and resulting estimates. Dots on top of station numbers represent station groups: "South" (light orange), "Guinea Dome-Cape Blanc" (green), "North" (violet). Data interpolation was performed with DIVA in Matlab (R2017a).

Prokaryotic biomass (Supplementary Fig. S4) was largely governed by cell abundances. Surface values increased from 5–7 μgC L^{-1} in the south to 15–20 μgC L^{-1} toward the Guinea Dome area, peaking at Cape Blanc at 36 μgC L^{-1}. As abundance patterns, while decreasing with depth, biomass also displayed a latitudinal gradient in both the mesopelagic and bathypelagic layers, producing significant positive relationships with Chl *a* in epi-, meso-, and bathypelagic layers (Table S3). Resulting archetype values for the Antarctic Intermediate Water of 5°C and the Subpolar Mode Water were 1.03 ± 0.09 and 1.49 ± 0.11 μgC L^{-1}, respectively, while in bathypelagic waters biomasses below 0.55 μgC L^{-1} in the south contrasted with values of 0.6–1 μgC L^{-1} in the north.

Surface communities were dominated by LNA cells (in many cases exceeding 65% of counts) except in Sta. 11 (Fig. 2b). An increase of HNA contribution was observed from the southern stations across the Guinea Dome area toward Cape Blanc. In the dark ocean, HNA prokaryotes overall dominated the community (Fig. 2b), their contribution increasing with depth and reaching > 65% in some bathypelagic samples. This was evident too from the different log–log slopes (Table 1), as the abundance of LNA prokaryotes

Table 1. Log–log regressions of prokaryotic abundances (as cells mL^{-1}) and leucine incorporation rates (as pmol Leu L^{-1} d^{-1}) vs depth, for samples of ≥ 10 m. Results are presented for the entire dataset ("all") and by station group: "South" (Stas. 1–7), "Guinea Dome-Cape Blanc" (8–11), and "North" (12–13, if available). *Slope* and *intercept* estimates are presented alongside 95% confidence intervals. r^2 is the adjusted coefficient of determination, *p* the p-value of the regression and *n* the number of samples per regression.

Variable	Station group	Slope	Intercept	r^2	*p*	*n*
HNA prokaryotes	All	−0.691±0.037	6.514±0.102	0.84	<0.001	261
	South	−0.661±0.039	6.328±0.108	0.89	<0.001	142
	Guine Dome-Cape Blanc	−0.724±0.055	6.742±0.151	0.90	<0.001	82
	North	−0.693±0.079	6.608±0.215	0.90	<0.001	37
LNA prokaryotes	All	−0.923±0.038	7.107±0.105	0.90	<0.001	261
	South	−0.953±0.049	7.107±0.136	0.91	<0.001	142
	Guinea Dome-Cape Blanc	−0.848±0.045	6.956±0.125	0.95	<0.001	82
	North	−0.921±0.076	7.307±0.207	0.94	<0.001	37
All prokaryotes	All	−0.816±0.035	7.149±0.096	0.89	<0.001	261
	South	−0.823±0.042	7.075±0.117	0.91	<0.001	142
	Guinea Dome-Cape Blanc	−0.783±0.045	7.153±0.124	0.94	<0.001	82
	North	−0.820±0.069	7.305±0.188	0.94	<0.001	37
Viable prokaryotes	All	−0.916±0.048	7.241±0.131	0.86	<0.001	231
	South	−0.950±0.050	7.204±0.140	0.92	<0.001	129
	Guinea Dome-Cape Blanc	−0.868±0.058	7.255±0.160	0.92	<0.001	82
	North	−0.870±0.118	7.354±0.322	0.93	<0.001	20
Leucine incorporation	All	−1.261±0.097	4.213±0.269	0.81	<0.001	152
	South	−1.331±0.122	4.447±0.342	0.83	<0.001	98
	Guinea Dome-Cape Blanc	−1.148±0.154	3.830±0.424	0.81	<0.001	54
	North	-	-	-	-	-

(−0.923 ± 0.038) decreased markedly faster than HNA prokaryotes (−0.691 ± 0.037). While HNA contribution in Sta. 11 was > 50% in the entire water column (with particularly high values [75%] at the bottom), in Stas. 12 and 13 HNA contributions were back below 50% (down to ∼ 1500 m). However, no significant relationship was observed between surface Chl *a* and average HNA % in the dark ocean, only the epipelagic layer showing a significant positive relationship (Fig. 3b; Supplementary Table S3).

The average cell volume (Fig. 2c) of prokaryotic communities was lowest in surface waters, with values of 0.030–0.060 μm^3 that were rather uniform along the entire cruise section, resulting in no significant relationship with Chl *a* concentrations (Fig. 3c; Supplementary Table S3). Cell volumes overall increased with depth, although with clear latitudinal differences: in Stas. 1–7 and 12–13, volumes of > 0.065 μm^3 were reached between 300–700 m depth, while in Stas. 8–11, such volumes were only present below 1200–1500 m. These latitudinal differences in deep waters were reflected in significant negative relationships with surface Chl *a* concentrations, both in the meso- and bathypelagic layers (Fig. 3c; Supplementary Table S3). This was also evident in archetype cell volumes of water masses, for example, the Antarctic Intermediate Water of 5°C and the Subpolar Mode Water presented values of 0.0710 ± 0.0035 and 0.0582 ± 0.0034 μm^3, respectively (Table 2). The highest average cell volumes were observed in bathypelagic waters of Stas. 1–7, most samples exceeding 0.090 μm^3 (some reaching > 0.15 μm^3).

The fraction of viable cells (presenting intact cell membranes) was highest in epipelagic waters with widespread > 70% contributions to the total number of detected cells and peaks exceeding 90% (Fig. 2d). Viability, however, consistently decreased with depth along the section (log–log slopes of − 0.916 ± 0.048, Table 1), following the opposite pattern to cell volume. Stas. 1–7 showed quick decreases in the abundance of viable cells (log–log slope = −0.950 ± 0.050; Supplementary Fig. S3; Table 1), with proportions < 70% immediately below the epipelagic layer, and < 50% below ∼ 1000 m in many samples, especially in Stas. 1–4. In Stas. 8–12, on the contrary (log–log slope in "Guinea Dome-Cape Blanc" = − 0.868 ± 0.058; Supplementary Fig. S3; Table 1), viabilities above 70% were measured down to ∼ 1000 m. This produced archetype viabilities of 61.4 ± 2.4% and 76.1 ± 2.4% for the Antarctic Intermediate Water of 5°C and the Subpolar Mode Water, respectively. This gradient along the section was consistent down to 3500 m, were values of 35–50% in Stas. 1–2 contrasted with viabilities > 70% in samples close to the bottom at Stas. 10–12. These changes yielded significant positive relationships between surface Chl *a* and cell viability in the meso- and bathypelagic waters (Fig. 3d; Supplementary Table S3).

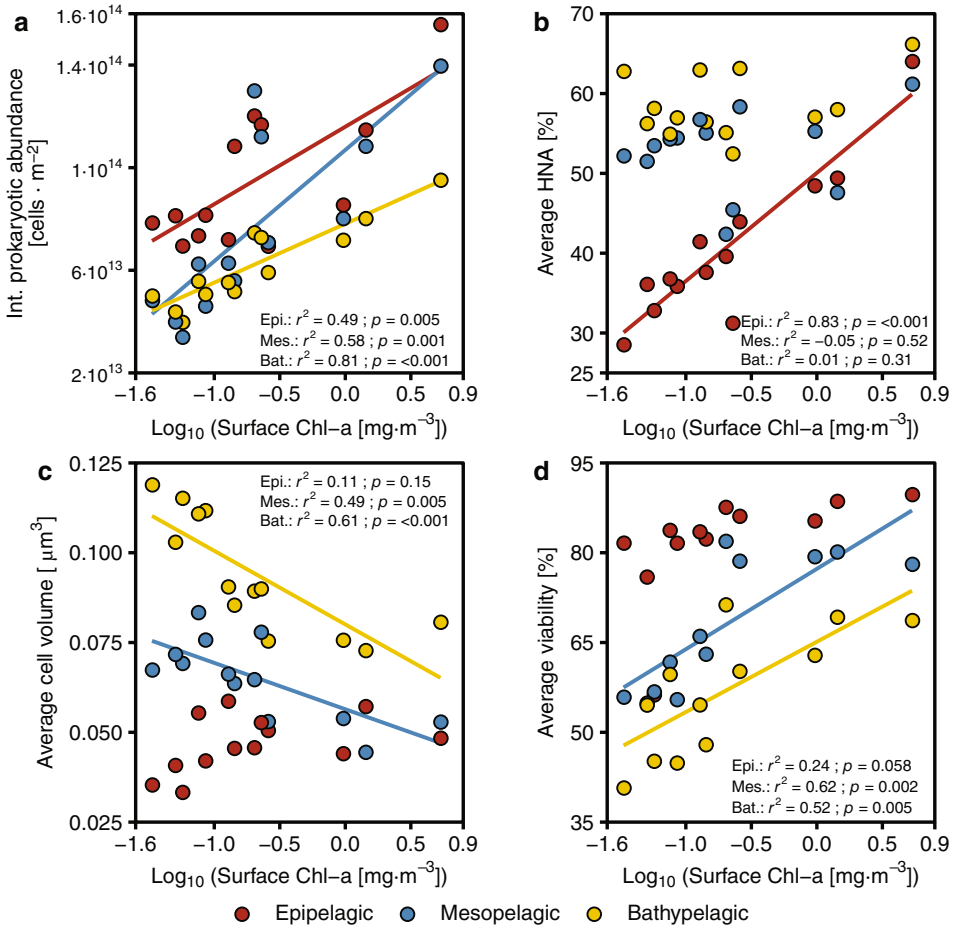

Fig. 3. Linear regressions between surface Chl *a* concentrations (averaged within the first 20 m, as proxy for productivity) and cytometric variables: (**a**) integrated prokaryotic abundance, (**b**) average HNA cell percentage, (**c**) average cell volume, and (**d**) average cell viability. Regressions estimated separately for epipelagic (≤ 200 m), mesopelagic (> 200 m and ≤ 1000 m), and bathypelagic (> 1000 m and ≤ 3000 m) layers. Regression lines are only shown for significant ($p < 0.05$) results. Regression parameters are presented in Table S3.

Epipelagic viability also displayed a positive relationship with surface Chl *a* (Fig. 3d), although it was not significant.

Leucine incorporation rates (Fig. 4a), a measure of prokaryotic activity, decreased drastically with depth (log–log slope = −1.261 ± 0.097; Table 1). Overall leucine incorporation rates were greater than 150 pmol Leu L^{-1} d^{-1} in the upper 50 m of the water column, with peaks at Stas. 4 (564 pmol Leu L^{-1} d^{-1}), 7 (420 pmol Leu L^{-1} d^{-1}), 9 (377 pmol Leu L^{-1} d^{-1}), and 11 (823 pmol Leu L^{-1} d^{-1}). Rates decreased to 15 pmol Leu L^{-1} d^{-1} by 300 m and to 2 pmol Leu L^{-1} d^{-1} by 1000–1500 m depth. No consistent latitudinal differences were observed in mesopelagic samples, but overall leucine incorporation rates in the bathypelagic were higher in the south, with the exception of samples close to the bottom at Stas. 9–11. Log–log slopes vs. depth in "South" and "Guinea Dome-Cape Blanc" stations, although different, had considerable confidence intervals (− 1.331 ± 0.122 and − 1.148 ± 0.154, respectively; Table 1), and no significant relationships were found between leucine incorporation rates and surface Chl *a* concentrations (Supplementary Fig. S5a; Supplementary Table S3).

Specific leucine incorporation rates per viable cell (Fig. 4b) tended to be higher in the southern end of the section. In epipelagic waters, specific rates were widely above 0.3×10^{-6} pmol Leu viable cell^{-1} d^{-1} in Stas. 1–5, with multiple samples exceeding 0.6 pmol Leu viable cell^{-1} d^{-1}. In Stas. 8–11, values were lower and barely exceed 0.3×10^{-6} pmol Leu viable cell^{-1} d^{-1}. In mesopelagic samples, specific leucine incorporation rates per viable cell ranged between $(0.06–0.3) \times 10^{-6}$ pmol Leu viable cell^{-1} d^{-1} and were slightly greater in the south, although no clear differences were observed between water masses (Subpolar Mode Water = $(0.103 \pm 0.029) \times 10^{-6}$ and Antarctic Intermediate Water of 5°C = $(0.228 \pm 0.070) \times 10^{-6}$ pmol Leu viable cell^{-1} d^{-1}, Table 2). As bulk leucine incorporation rates, viable cell-specific rates in bathypelagic waters tended to increase towards the south, overall exceeding 0.06×10^{-6} pmol Leu viable cell^{-1} d^{-1}, while Stas. 8–11 mostly showed specific

Table 2. Characterization of the prokaryotic community in the water masses. Contribution of each water mass to the total sampled volume (as %), and archetype values (± standard error) of depth, latitude, and biological parameters. Water mass acronyms stand for: salinity maximum water (SMW), Madeira mode water (MMW), equatorial water (EQ_{13}), eastern North Atlantic central water of 15°C ($ENACW_{15}$) and 12°C ($ENACW_{12}$), subpolar mode water (SPMW), Mediterranean water (MW), Antarctic intermediate water of 5°C ($AAIW_5$) and 3.1°C ($AAIW_{3.1}$), circumpolar deep water (CDW), and North Atlantic deep water of 4.6°C ($NADW_{4.6}$) and 2°C ($NADW_2$).

Water mass	Volume (%)	Depth (m)	Latitude (°N)	Prokaryotic abundance* (cell mL^{-1})	HNA (%)	Cell viability (%)	Cell volume† (μm^3)	Prokaryotic biomass ($\mu gC\ L^{-1}$)	Leucine incorporation (pmol Leu L^{-1} d^{-1})	Specific leucine incorporation‡ (pmol Leu viable $cell^{-1}$ d^{-1})
SMW	2.88	134±11	−9.68±1.80	27.4±3.2	31.0±3.2	69.4±6.8	38.1±4.1	3.350±0.386	103.93±39.15	0.759±0.449
MMW	1.95	130±17	22.13±2.67	38.0±5.6	46.5±5.9	89.0±1.7	50.4±7.2	5.692±1.110	27.77±13.02	0.092±0.056
EQ_{13}	15.71	252±23	3.13±1.66	15.7±1.4	53.7±1.7	74.3±2.2	50.7±1.9	2.195±0.165	33.11±11.45	0.290±0.119
$ENACW_{15}$	2.09	186±34	25.40±1.07	35.3±4.8	44.3±4.2	86.9±1.8	54.1±5.8	5.527±0.934	23.33±34.45	0.072±0.166
$ENACW_{12}$	4.68	413±53	22.40±1.26	21.0±2.4	52.8±3.2	84.1±2.2	57.1±5.0	3.186±0.265	15.16±7.38	0.072±0.043
SPMW	8.34	696±56	17.32±1.39	9.5±0.8	52.4±1.9	76.1±2.4	58.2±3.4	1.493±0.114	7.58±1.89	0.103±0.029
MW	0.76	1632±386	25.28±1.68	4.7±1.1	54.7±6.9	70.8±5.2	85.8±12.5	0.974±0.257	1.65±1.73	0.042±0.033
$AAIW_5$	12.83	713±47	0.22±1.86	5.8±0.5	53.7±1.0	61.4±2.4	71.0±3.5	1.034±0.086	6.34±1.48	0.228±0.070
$AAIW_{3.1}$	0.3	1052±315	−9.26±6.56	3.0±0.6	55.9±6.5	50.1±9.8	86.7±25.6	0.632±0.201	4.01±4.00	0.311±0.319
CDW	5.89	1917±232	3.92±3.47	3.2±0.3	58.3±1.8	56.1±3.7	93.9±6.8	0.695±0.072	1.99±0.94	0.140±0.069
$NADW_{4.6}$	30	1485±75	5.99±1.46	3.9±0.2	56.6±0.9	59.3±1.8	83.9±2.7	0.781±0.038	2.45±0.65	0.126±0.031
$NADW_2$	14.57	2754±98	4.66±2.12	2.6±0.2	61.7±1.0	55.7±2.3	107.8±5.4	0.646±0.058	1.08±0.13	0.086±0.013

*$\times 10^4$.
†$\times 10^{-3}$.
‡$\times 10^{-6}$.

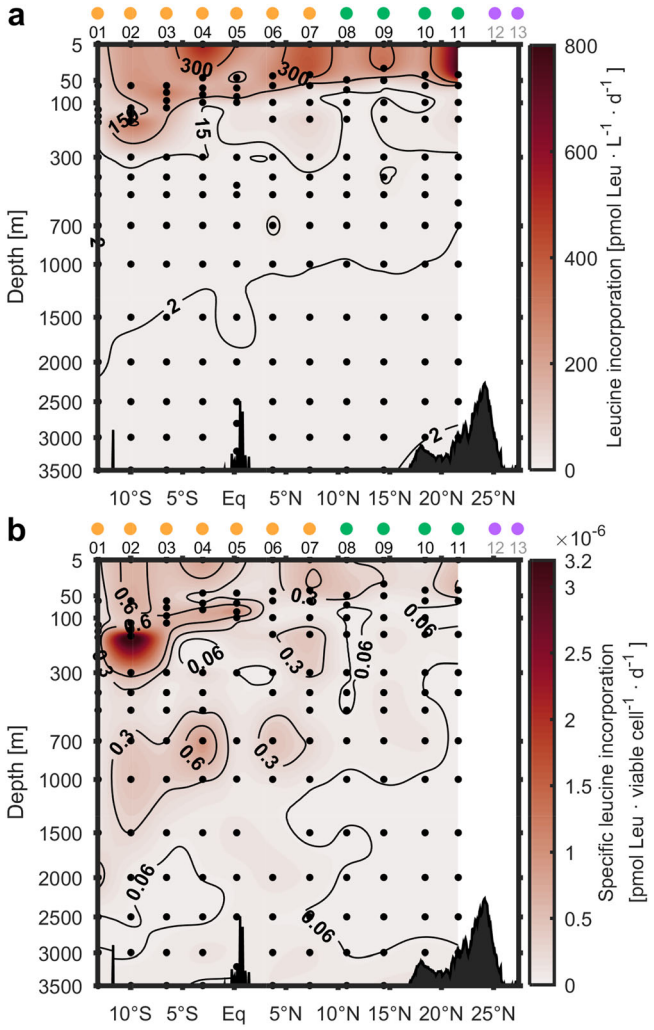

Fig. 4. Prokaryotic activity as leucine incorporation rates. (**a**) Bulk leucine incorporation rate, (**b**) specific leucine incorporation rate per viable cell (contour lines are in 10^{-6}). Black dots represent locations of collected samples and resulting estimates. Dots on top of station numbers represent station groups: "South" (light orange), "Guinea Dome-Cape Blanc" (green), "North" (violet). Data interpolation was performed with DIVA in Matlab (R2017a).

rates below 0.06×10^{-6} pmol Leu viable cell^{-1} d^{-1}, except samples close to the bottom. Average viable cell-specific rates in bathypelagic waters did show a (weak) negative relationship with surface Chl *a* (Supplementary Fig. S5b; Supplementary Table S3).

Discussion

The oceanographic section studied encompassed widely diverse environments along the tropical and subtropical Atlantic, from the oligotrophic tropical south Atlantic to the highly productive waters of the Cape Blanc area in the Northwest African upwelling system (Fig. 1a; Carr and Kearns 2003). The transition from waters of low to high productivity was well captured by the increasing concentrations of Chl *a* measured in epipelagic waters from Stas. 1 to 11, along with a shoaling of the DCM (Fig. 1b). In a previous work with data collected during the same cruise, we reported intense fluorescence signals of protein-like dissolved organic matter at Stas. 8, 9, 11, and 12 for the entire water column (Gómez-Letona et al. 2022*d*). These findings suggest vertical transport of organic matter from the surface into the dark ocean in the Guinea Dome-Cape Blanc region, in agreement with previous studies with sediment traps reporting high sinking particle fluxes (Fischer et al. 2020).

Observed prokaryotic abundances (Fig. 2a) were in the range of those previously described in the eastern tropical and subtropical North Atlantic for epipelagic (> 10^5 cells mL^{-1}), mesopelagic (10^4–10^5 cells mL^{-1}), and bathypelagic (10^4 cells mL^{-1}) waters (Varela et al. 2008; Baltar et al. 2010*b*, 2012). The vertical decrease in cell abundances of the different prokaryotic groups (total, LNA, HNA), evaluated with log–log relationship vs. depth (Table 1), yielded slope values that were in the range of those reported in the literature (Arístegui et al. 2009; Gasol et al. 2009). HNA and LNA groups had markedly different slopes, which resulted in increases in the relative contribution of HNA cells with depth. Prokaryotic cell volume increase with depth has also been documented before, although our estimated cell volumes were higher (La Ferla et al. 2012, 2015) or lower (Morán et al. 2015) than previous observations. The increases in the proportion of HNA prokaryotes and cell volume with depth agree with previous studies (Van Wambeke et al. 2011; La Ferla et al. 2012), and can be interpreted as an increase in the contribution of larger prokaryotic cells, with bigger genomes (Bouvier et al. 2007). The homogeneous profile of high % of HNA cells (> 60%) observed close to Cape Blanc (Fig. 2b, Sta. 11) was similar to the profile reported by Gasol et al. (2009) for the same area and points to the presence of copiotrophic taxa in the epipelagic waters mostly influenced by the upwelling system. HNA cells have also been related to higher activity (Servais et al. 2003), which would go in line with the very high leucine incorporation measured in Sta. 11 (Fig. 4a).

Descriptions of prokaryotic viability in the deep ocean are scarce and this is, to the best of the authors' knowledge, the most extensive study of cell viabilities in a large-scale sampling effort that includes bathypelagic samples. The relative contribution of viable prokaryotes to total counts in epipelagic waters (> 80%, Fig. 2d) was similar to prior estimates within the eastern subtropical North Atlantic (Baltar et al. 2012). A previous study in the eastern subtropical Atlantic showed a positive relationship between epipelagic viability of prokaryotes and the release of organic matter by senescent phytoplankton, which was higher in oligotrophic waters (Lasternas and Agustí 2014). Here, lower values were observed in waters with low productivity, although no significant linear relationship was found between cell viability in epipelagic waters and

surface Chl *a*. Out of the epipelagic layer, trends of vertical decreases in prokaryotic viability have been documented, with viability values as low as 10–40% (Gasol et al. 2009; Baltar et al. 2012), comparable to the minimum values observed here in the southern end of the section. This vertical trend points to harsher conditions (low temperature, high pressure, reduced dissolved organic matter availability) for prokaryotes in deep ocean environments (Herndl and Reinthaler 2013). While depressurization during sample collection could have an effect in cell viability, we considered this effect to be minimal as samples were analyzed before the change in pressure could have had a significant negative impact on cell membranes (Quéric et al. 2004, see Methods section for further information).

In the deep ocean, cell viability, abundance, and volume displayed latitudinal trends matching surface productivity gradients (as defined by Chl *a* concentrations; Fig. 3). The tendency to more abundant, more viable, and smaller cells in the mesopelagic and bathypelagic layers under highly productive surface waters with important vertical flux of particles (Fischer et al. 2020) suggests a remarkable effect of sinking particles in the prokaryotic communities of the dark ocean. While a link between surface productivity and abundance/biomass of deep ocean prokaryotes has been found before (Hansell and Ducklow 2003; Yokokawa et al. 2013), our results demonstrate that surface productivity also exerts a major imprint on their physiological status. The effect of vertical connectivity would be twofold, including the transport of both resources and microorganisms. Sinking particles would introduce organic matter, including its release by senescent phytoplankton cells (Lasternas and Agustí 2014; Agustí et al. 2015), fuelling prokaryotes and allowing them to attain higher viabilities. Besides the well-known high particle fluxes in the Northwestern African upwelling area (Fischer et al. 2020), this vertical input was further suggested by the correspondence between meso- and bathypelagic protein-like fluorescent dissolved organic matter (resembling peak T, Coble 1996) and surface productivity proxies in the study area (Gómez-Letona et al. 2022*d*), in a similar manner to other oceanic regions (Ruiz-González et al. 2020). Moreover, the sinking particles could also act as vectors, transporting particle-attached prokaryotes from epipelagic communities to the dark ocean, yielding communities more similar to each other than in regions with low vertical transport (Mestre et al. 2018). This could also help explain the smaller size of deep ocean prokaryotes under the more productive stations. The changes in viability of deep ocean prokaryotes under different productivity regimes have important implications. The assessment of the physiological status of individual cells (whether they are dead or alive, or displaying various degrees of activity) is key to correctly understand processes at the community level (Sebastián and Gasol 2019). Our estimates indicate that the metabolic processes in meso- and bathypelagic waters are not driven by the entire community, only by a varying fraction of it, which will depend on the surface productivity regime. This underlines the importance of considering a wide oceanographic context when studying dark ocean prokaryotes.

The magnitude of leucine incorporation rates in the epipelagic (10^1–10^2 pmol Leu L^{-1} d^{-1}), mesopelagic (10^0–10^1 pmol Leu L^{-1} d^{-1}) and bathypelagic layers (10^{-1}–10^0 pmol Leu·L^{-1} d^{-1}) was in the same range as previous studies in the eastern subtropical and tropical North Atlantic (Varela et al. 2008; De Corte et al. 2010). The log–log slope for the entire dataset was also similar to other slopes reported in the literature for the global ocean (Arístegui et al. 2009). An exception to the decreasing rates of leucine incorporation with depth was found in samples close to the bottom at Stas. 9–11, which showed relatively high rates that might have been fuelled by resuspension (Fischer et al. 2009; Ziervogel et al. 2016) or by the arrival of fast sinking particles (Boeuf et al. 2019). We found absent (for bulk rates) or negative (for cell-specific rates in the bathypelagic) relationships between surface productivity and leucine incorporation in the dark ocean (Supplementary Fig. S5; Supplementary Table S3), manifesting that, while the vertical connection between surface productivity and prokaryotic viability was evident, the connection with heterotrophic activity was unclear. These findings are in line with previous studies that found positive but weak relationships between vertical particle flux and prokaryotic production in the mesopelagic, but none in the bathypelagic (Yokokawa et al. 2013).

The unclear relationship between surface productivity and prokaryotic heterotrophic activity may be due to methodological limitations, since prokaryotic production is estimated from metabolic rates, but sometimes metabolism might not be directed to cell-growth but to cell maintenance (Carlson et al. 2007; Giering and Evans 2022). Particularly in hostile environmental conditions, with low resources and energy supply, prokaryotes have been found to achieve lower growth efficiencies (del Giorgio and Cole 1998). In these situations, resources and energy are directed in greater proportions to the maintenance of cell structures and functionality, instead of biomass production and growth (Carlson et al. 2007). The bathypelagic waters of Stas. 1–4 showed minimum cell viability ratios, in agreement with expected harsher conditions due to potential low external inputs of organic substrates in these oligotrophic waters. The relatively high specific leucine incorporation rates in the deep waters of these southern stations might thus be linked to metabolism directed to maintenance, rather than growth and cell division. Moreover, larger prokaryotes have greater metabolic requirements than smaller ones (del Giorgio and Gasol 2008), and we indeed found that high average values of specific leucine incorporation in the bathypelagic were associated with high average cell sizes (Figs. 2, 3, S6). There is increasing evidence that leucine-to-carbon conversion factors are highly variable in the ocean, decreasing with depth and increasing with water productivity (del Giorgio and Cole 1998; Orta-Ponce et al. 2021; Giering and

Evans 2022). Considering these trends, the negative relationship between leucine incorporation in bathypelagic samples and surface productivity would not directly translate to prokaryotic heterotrophic production, as lower conversion factors could be expected in the southern stations relative to the Guinea Dome-Cape Blanc area. This would potentially result in higher production rates under the productive waters, which would agree with the other trends of increased viability and cell numbers. Thus, variations in the leucine-to-carbon conversion factors probably explain the lack of relationship between surface productivity and prokaryotic heterotrophic activity (as measured by leucine incorporation) in the dark realm.

Conclusions

We studied the abundance, cell size, viability, and heterotrophic metabolism of prokaryotic communities from surface down to 3500 m depth along a primary productivity gradient in the subtropical and tropical Atlantic. Our results show that deeper waters tended to harbor communities with reduced cell concentrations and viability, but larger cell sizes and high nucleic acid content. The trends were coupled with changes along surface productivity: waters under highly productive areas presented higher cell counts and viability, and lower average cell sizes, than waters under oligotrophic zones. These relationships were significant down to the bathypelagic zone (and were reflected in the archetype values of water masses), highlighting the extent of the vertical connectivity along the water column. The heterotrophic metabolism, however, was not equally affected: while bulk leucine incorporation rates displayed no significant relationship with surface productivity, cell-specific rates showed a negative relationship in bathypelagic waters. Energy and resource allocation to cellular maintenance processes under adverse environmental conditions (likely resulting in low conversion of the incorporated leucine into biomass), and dependence of metabolic requirements on cell size could influence the conversion of leucine incorporation into carbon production. Our work provides further evidence on the link between the productivity regime of surface waters and dark ocean processes. The effect of surface productivity on the viability of dark ocean prokaryotes is particularly relevant, as the physiological status of the prokaryotes will determine who drives metabolic processes at the community level and, hence, dark ocean biogeochemical cycles.

Data availability statement

The data used in this study are available in the PANGAEA repository (pangaea.de) under accession numbers 943414 and 943416 (Gómez-Letona et al. 2022*a*,*b*,*c*).

References

Agustí, S., J. I. González-Gordillo, D. Vaqué, M. Estrada, M. I. Cerezo, G. Salazar, J. M. Gasol, and C. M. Duarte. 2015. Ubiquitous healthy diatoms in the deep sea confirm deep carbon injection by the biological pump. Nat. Commun. **6**: 7608. doi:10.1038/ncomms8608

Álvarez, M., S. Brea, H. Mercier, and X. A. Álvarez-Salgado. 2014. Mineralization of biogenic materials in the water masses of the South Atlantic Ocean. I: Assessment and results of an optimum multiparameter analysis. Prog. Oceanogr. **123**: 1–23. doi:10.1016/j.pocean.2013.12.007

Álvarez-Salgado, X. A., M. Nieto-Cid, M. Álvarez, F. F. Pérez, P. Morin, and H. Mercier. 2013. New insights on the mineralization of dissolved organic matter in central, intermediate, and deep water masses of the Northeast North Atlantic. Limnol. Oceanogr. **58**: 681–696. doi:10.4319/lo.2013.58.2.0681

Arístegui, J., J. M. Gasol, C. M. Duarte, and G. J. Herndl. 2009. Microbial oceanography of the dark ocean's pelagic realm. Limnol. Oceanogr. **54**: 1501–1529. doi:10.4319/lo.2009.54.5.1501

Baltar, F., J. Arístegui, J. M. Gasol, I. Lekunberri, and G. J. Herndl. 2010*a*. Mesoscale eddies: Hotspots of prokaryotic activity and differential community structure in the ocean. ISME J. **4**: 975–988. doi:10.1038/ismej.2010.33

Baltar, F., J. Arístegui, J. M. Gasol, E. Sintes, H. M. Van Aken, and G. J. Herndl. 2010*b*. High dissolved extracellular enzymatic activity in the deep Central Atlantic Ocean. Aquat. Microb. Ecol. **11**: 1998–2014. doi:10.3354/ame01377

Baltar, F., J. Arístegui, E. Sintes, J. M. Gasol, T. Reinthaler, and G. J. Herndl. 2010*c*. Significance of non-sinking particulate organic carbon and dark CO 2 fixation to heterotrophic carbon demand in the mesopelagic Northeast Atlantic. Geophys. Res. Lett. **37**: L09602. doi:10.1029/2010GL043105

Baltar, F., J. Arístegui, J. M. Gasol, and G. J. Herndl. 2012. Microbial functioning and community structure variability in the mesopelagic and epipelagic waters of the subtropical Northeast Atlantic Ocean. Appl. Environ. Microbiol. **78**: 3309–3316. doi:10.1128/AEM.07962-11

Bar-On, Y. M., R. Phillips, and R. Milo. 2018. The biomass distribution on Earth. Proc. Natl. Acad. Sci **115**: 6506–6511. doi:10.1073/pnas.1711842115

Boeuf, D., and others. 2019. Biological composition and microbial dynamics of sinking particulate organic matter at abyssal depths in the oligotrophic open ocean. Proc. Natl. Acad. Sci. **116**: 11824–11832. doi:10.1073/pnas.1903080116

Bouvier, T., P. A. Del Giorgio, and J. M. Gasol. 2007. A comparative study of the cytometric characteristics of high and low nucleic-acid bacterioplankton cells from different aquatic ecosystems. Environ. Microbiol. **9**: 2050–2066. doi:10.1111/j.1462-2920.2007.01321.x

Boyd, P. W., H. Claustre, M. Levy, D. A. Siegel, and T. Weber. 2019. Multi-faceted particle pumps drive carbon sequestration in the ocean. Nature **568**: 327–335. doi:10.1038/s41586-019-1098-2

Brandt, P., V. Hormann, B. Bourlès, J. Fischer, F. A. Schott, L. Stramma, and M. Dengler. 2008. Oxygen tongues and

zonal currents in the equatorial Atlantic. J. Geophys. Res. Ocean. **113**: C04012. doi:10.1029/2007JC004435

Broecker, W. S. 1974. "NO", a conservative water-mass tracer. Earth Planet. Sci. Lett. **23**: 100–107. doi:10.1016/0012-821X(74)90036-3

Calvo-Díaz, A., and X. A. G. Morán. 2006. Seasonal dynamics of picoplankton in shelf waters of the southern Bay of Biscay. Aquat. Microb. Ecol. **42**: 159–174. doi:10.3354/ame042159

Carlson, C. A., P. A. del Giorgio, and G. J. Herndl. 2007. Microbes and the dissipation of energy and respiration: From cells to ecosystems. Oceanography **20**: 89–100.

Carr, M. E., and E. J. Kearns. 2003. Production regimes in four eastern boundary current systems. Deep-Sea Res. Part II Top. Stud. Oceanogr. **50**: 3199–3221. doi:10.1016/j.dsr2.2003.07.015

Catalá, T. S., and others. 2015. Turnover time of fluorescent dissolved organic matter in the dark global ocean. Nat. Commun. **6**: 5986. doi:10.1038/ncomms6986

Coble, P. G. 1996. Characterization of marine and terrestrial DOM in seawater using excitation-emission matrix spectroscopy. Mar. Chem. **51**: 325–346. doi:10.1016/0304-4203(95)00062-3

De Corte, D., E. Sintes, C. Winter, T. Yokokawa, T. Reinthaler, and G. J. Herndl. 2010. Links between viral and prokaryotic communities throughout the water column in the (sub) tropical Atlantic Ocean. ISME J. **4**: 1431–1442. doi:10.1038/ismej.2010.65

del Giorgio, P. A., and J. J. Cole. 1998. Bacterial growth efficiency in natural aquatic systems. Annu. Rev. Ecol. Syst. **29**: 503–541. doi:10.1146/annurev.ecolsys.29.1.503

del Giorgio, P. A., and J. M. Gasol. 2008. Physiological structure and single-cell activity in marine Bacterioplankton, p. 243–298. *In* D. L. Kirchman [ed.], Microbial ecology of the oceans. John Wiley & Sons.

Falcioni, T., S. Papa, and J. M. Gasol. 2008. Evaluating the flow-cytometric nucleic acid double-staining protocol in realistic situations of planktonic bacterial death. Appl. Environ. Microbiol. **74**: 1767–1779. doi:10.1128/AEM.01668-07

Fischer, G., and others. 2020. Long-term changes of particle flux in the Canary Basin between 1991 and 2009 and comparison to sediment trap records off Mauritania. Front. Earth Sci. **8**: 280. doi:10.3389/feart.2020.00280

Fischer, G., C. Reuter, G. Karakas, N. Nowald, and G. Wefer. 2009. Offshore advection of particles within the Cape Blanc filament, Mauritania: Results from observational and modelling studies. Prog. Oceanogr. **83**: 322–330. doi:10.1016/j.pocean.2009.07.023

Gasol, J. M., L. Alonso-Sáez, D. Vaqué, F. Baltar, M. L. Calleja, C. M. Duarte, and J. Arístegui. 2009. Mesopelagic prokaryotic bulk and single-cell heterotrophic activity and community composition in the NW Africa-Canary Islands coastal-transition zone. Prog. Oceanogr. **83**: 189–196. doi:10.1016/j.pocean.2009.07.014

Giering, S. L. C., and C. Evans. 2022. Overestimation of prokaryotic production by leucine incorporation—And how to avoid it. Limnol. Oceanogr **67**: 725–738. doi:10.1002/lno.12032

Gómez-Letona, M., J. Arístegui, N. Hernández-Hernández, M. Pérez-Lorenzo, X. A. Alvarez-Salgado, E. Teira, and M. Sebastian. 2022*a*. Abundance, cell volume, biomass, viability and leucine incorporation rates of prokaryotes from the MAFIA cruise to the tropical and subtropical Atlantic in 2015. PANGAEA. doi:10.1594/PANGAEA.943417

Gómez-Letona, M., J. Arístegui, N. Hernández-Hernández, M. Pérez-Lorenzo, X. A. Alvarez-Salgado, E. Teira, and M. Sebastian. 2022*b*. Abundance, cell volume, biomass, viability and leucine incorporation rates of prokaryotes in the tropical and subtropical Atlantic. PANGAEA. doi:10.1594/PANGAEA.943414

Gómez-Letona, M., J. Arístegui, N. Hernández-Hernández, M. Pérez-Lorenzo, X. A. Alvarez-Salgado, E. Teira, and M. Sebastian. 2022*c*. Integrated abundance, cell volume, viability and leucine incorporation rates of prokaryotes in the epipelagic, mesopelagic and bathypelagic layers of the tropical and subtropical Atlantic. PANGAEA. doi:10.1594/PANGAEA.943416

Gómez-Letona, M., and others. 2022*d*. Deep ocean prokaryotes and fluorescent dissolved organic matter reflect the history of the water masses across the Atlantic Ocean. Prog. Oceanogr. **205**: 102819. doi:10.1016/j.pocean.2022.102819

Guidi, L., L. Stemmann, G. A. Jackson, F. Ibanez, H. Claustre, L. Legendre, M. Picheral, and G. Gorskya. 2009. Effects of phytoplankton community on production, size, and export of large aggregates: A world-ocean analysis. Limnol. Oceanogr. **54**: 1951–1963. doi:10.4319/lo.2009.54.6.1951

Hansell, D. A., and H. W. Ducklow. 2003. Bacterioplankton distribution and production in the bathypelagic ocean: Directly coupled to particulate organic carbon export? Limnol. Oceanogr. **48**: 150–156. doi:10.4319/lo.2003.48.1.0150

Herndl, G. J., and T. Reinthaler. 2013. Microbial control of the dark end of the biological pump. Nat. Geosci. **6**: 718–724. doi:10.1038/ngeo1921

Kirchman, D., E. K'nees, and R. Hodson. 1985. Leucine incorporation and its potential as a measure of protein synthesis by bacteria in natural aquatic systems. Appl. Environ. Microbiol. **49**: 599–607. doi:10.1128/AEM.67.4.1775-1782.2001

La Ferla, R., G. Maimone, M. Azzaro, F. Conversano, C. Brunet, A. S. Cabral, and R. Paranhos. 2012. Vertical distribution of the prokaryotic cell size in the Mediterranean Sea. Helgol. Mar. Res. **66**: 635–650. doi:10.1007/s10152-012-0297-0

La Ferla, R., G. Maimone, A. Lo Giudice, F. Azzaro, A. Cosenza, and M. Azzaro. 2015. Cell size and other phenotypic traits of prokaryotic cells in pelagic areas of the Ross Sea (Antarctica). Hydrobiologia **761**: 181–194. doi:10.1007/s10750-015-2426-7

Lasternas, S., and S. Agustí. 2014. The percentage of living bacterial cells related to organic carbon release from senescent oceanic phytoplankton. Biogeosciences **11**: 6377–6387. doi:10.5194/bg-11-6377-2014

Mestre, M., C. Ruiz-González, R. Logares, C. M. Duarte, J. M. Gasol, and M. M. Sala. 2018. Sinking particles promote vertical connectivity in the ocean microbiome. Proc. Natl. Acad. Sci. USA **115**: E6799–E6807. doi:10.1073/pnas.1802470115

Moran, M. A. 2015. The global ocean microbiome. Science **350**: aac8455. doi:10.1126/science.aac8455

Morán, X. A. G., and others. 2015. More, smaller bacteria in response to ocean's warming? Proc. R. Soc. B Biol. Sci. **282**: 20150371. doi:10.1098/rspb.2015.0371

Norland, S. 1993. The relationship between biomass and volume of bacteria, p. 303–307. *In* P. F. Kemp, B. F. Sherr, E. B. Sherr, and J. J. Cole [eds.], Handboook of methods in aquatic microbial ecology. Lewis Publishers.

Orta-Ponce, C. P., T. Rodríguez-Ramos, M. Nieto-Cid, E. Teira, E. Guerrero-Feijóo, A. Bode, and M. M. Varela. 2021. Empirical leucine-to-carbon conversion factors in North-Eastern Atlantic waters (50–2000 m) shaped by bacterial community composition and optical signature of DOM. Sci. Rep. **11**: 24370. doi:10.1038/s41598-021-03790-y

Park, C. B., and D. S. Clark. 2002. Rupture of the cell envelope by decompression of the deep-sea methanogen *Methanococcus jannaschii*. Appl. Environ. Microbiol. **68**: 1458–1463. doi:10.1128/AEM.68.3.1458-1463.2002

Pérez, F. F., and others. 2001. Mixing analysis of nutrients, oxygen and inorganic carbon in the Canary Islands region. J. Mar. Syst. **28**: 183–201. doi:10.1016/S0924-7963(01)00003-3

Quéric, N.-V., T. Soltwedel, and W. E. Arntz. 2004. Application of a rapid direct viable count method to deep-sea sediment bacteria. J. Microbiol. Methods **57**: 351–367. doi:10.1016/j.mimet.2004.02.005

R Core Team. 2019. R: A language and environment for statistical computing. R Foundation for Statistical Computing, Vienna, Austria. https://www.R-project.org/.

Ruiz-González, C., and others. 2020. Major imprint of surface plankton on deep ocean prokaryotic structure and activity. Mol. Ecol. **29**: 1820–1838. doi:10.1111/mec.15454

Santana-Falcón, Y., E. Mason, and J. Arístegui. 2020. Offshore transport of organic carbon by upwelling filaments in the Canary Current system. Prog. Oceanogr. **186**: 102322. doi:10.1016/j.pocean.2020.102322

Sebastián, M., and J. M. Gasol. 2019. Visualization is crucial for understanding microbial processes in the ocean. Philos. Trans. R. Soc. B Biol. Sci. **374**: 20190083. doi:10.1098/rstb.2019.0083

Servais, P., E. O. Casamayor, C. Courties, P. Catala, N. Parthuisot, and P. Lebaron. 2003. Activity and diversity of bacterial cells with high and low nucleic acid content. Aquat. Microb. Ecol. **33**: 41–51. doi:10.3354/ame033041

Smith, D., and F. Azam. 1992. A simple, economical method for measuring bacterial protein synthesis rates in seawater using ^{3}H-leucine. Mar. Microb. Food Webs **6**: 107–114.

Smith, L. K., A. H. Ruhl, L. C. Huffard, M. Messié, and M. Kahru. 2018. Episodic organic carbon fluxes from surface ocean to abyssal depths during long-term monitoring in NE Pacific. Proc. Natl. Acad. Sci. **115**: 12235–12240. doi:10.1073/pnas.1814559115

Steinberg, D. K., B. A. S. Van Mooy, K. O. Buesseler, P. W. Boyd, T. Kobari, and D. M. Karl. 2008. Bacterial vs. zooplankton control of sinking particle flux in the ocean's twilight zone. Limnol. Oceanogr. **53**: 1327–1338. doi:10.4319/lo.2008.53.4.1327

Stramma, L., and F. Schott. 1999. The mean flow field of the tropical Atlantic Ocean. Deep-Sea Res. Part II Top. Stud. Oceanogr. **46**: 279–303. doi:10.1016/S0967-0645(98)00109-X

Troupin, C., and others. 2012. Generation of analysis and consistent error fields using the Data Interpolating Variational Analysis (DIVA). Ocean Model. **52–53**: 90–101. doi:10.1016/j.ocemod.2012.05.002

Turner, J. T. 2015. Zooplankton fecal pellets, marine snow, phytodetritus and the ocean's biological pump. Prog. Oceanogr. **130**: 205–248. doi:10.1016/j.pocean.2014.08.005

Van Wambeke, F., P. Catala, M. Pujo-Pay, and P. Lebaron. 2011. Vertical and longitudinal gradients in HNA-LNA cell abundances and cytometric characteristics in the Mediterranean Sea. Biogeosciences **8**: 1853–1863. doi:10.5194/bg-8-1853-2011

Varela, M. M., H. M. Van Aken, E. Sintes, and G. J. Herndl. 2008. Latitudinal trends of Crenarchaeota and bacteria in the meso- and bathypelagic water masses of the eastern North Atlantic. Environ. Microbiol. **10**: 110–124. doi:10.1111/j.1462-2920.2007.01437.x

Verdugo, P. 2012. Marine microgels. Ann. Rev. Mar. Sci. **4**: 375–400. doi:10.1146/annurev-marine-120709-142759

Whitman, W. B., D. C. Coleman, and W. J. Wiebe. 1998. Prokaryotes: The unseen majority. Proc. Natl. Acad. Sci **95**: 6578–6583. doi:10.1073/pnas.95.12.6578

Yokokawa, T., Y. Yang, C. Motegi, and T. Nagata. 2013. Large-scale geographical variation in prokaryotic abundance and production in meso- and bathypelagic zones of the Central Pacific and Southern Ocean. Limnol. Oceanogr. **58**: 61–73. doi:10.4319/lo.2013.58.1.0061

Ziervogel, K., and others. 2016. Enhanced particle fluxes and heterotrophic bacterial activities in Gulf of Mexico bottom waters following storm-induced sediment resuspension. Deep-Sea Res. Part II Top. Stud. Oceanogr. **129**: 77–88. doi:10.1016/j.dsr2.2015.06.017

Acknowledgments

The authors would like to thank the officers and crew of the *R/V Hespérides*, and the staff of the Unit of Marine Technology (UTM) of the Spanish Research Council (CSIC) for their invaluable help at sea. This work is a contribution to projects MAFIA (grant number CTM2012-39587-C04-01), FLUXES (grant number CTM2015-69392-C3), e-IMPACT (grant number

PID2019-109084RB-C21 and -C22), and INTERES (CTM2017-83362-R) funded by the Spanish "Plan Nacional/Estatal de I+D" and cofounded with FEDER funds, and to project SUMMER (grant number AMD-817806-5) funded by the European Union's Horizon 2020 research and innovation program. Markel Gómez-Letona is supported by the Ministerio de Ciencia, Innovación y Universidades, Gobierno de España (grant number FPU17-01435) during his PhD. Marta Sebastián is supported by the Project MIAU (grant number RTI2018-101025-B-I00) and the "Severo Ochoa Centre of Excellence" accreditation (CEX2019-000928-S).

Conflict of Interest

None declared.

Submitted 21 March 2022
Revised 05 September 2022
Accepted 01 October 2022

Associate editor: Hans-Peter Grossart